Supplementary Information

—

Observation and Manipulation of Chiral Phasons in a Magnetic System

Yang Wu*,[1,2] Chenhao Zhang*,[1] Jingyi Chen*,[1,2] Haonan Jin†,[1,2] Gerrit van der Laan,[3] Thorsten Hesjedal,[4] Yizhou Liu,[5] Jiadong Zang,[6] Xiaoping Liu†,[1] and Shilei Zhang†[1,2,7]

[1]*School of Physical Science and Technology, ShanghaiTech University, Shanghai 201210, China*

[2]*ShanghaiTech Laboratory for Topological Physics, ShanghaiTech University, Shanghai 201210, China*

[3]*Magnetic Spectroscopy, Diamond Light Source, Harwell Science and Innovation Campus, Didcot OX11 0DE, United Kingdom*

[4]*Department of Physics, Clarendon Laboratory, University of Oxford, Oxford OX1 3PU, United Kingdom*

[5]*Anhui Province Key Laboratory of Low-Energy Quantum Materials and Devices, High Magnetic Field Laboratory, HFIPS, Chinese Academy of Sciences, Hefei 230031, China*

[6]*Department of Physics and Astronomy, University of New Hampshire, Durham, NH, 03824, USA*

[7]*Center for Transformative Science, ShanghaiTech University, Shanghai 200031, China*

S1. MICROMAGNETIC SIMULATIONS

Micromagnetic simulations were performed using MUMAX3 on a $20 \times 20 \times 200$ mesh with $4 \times 4 \times 4\,\mathrm{nm}^3$ cubic cells. Material parameters specific to Cu_2OSeO_3 were used: exchange stiffness $A_{\mathrm{ex}} = 3.547 \times 10^{-13}$ J/m, Dzyaloshinskii–Moriya interaction strength $D = 7.42 \times 10^{-5}$ J/m^2, saturation magnetization $M_s = 1.044 \times 10^5$ A/m, and Gilbert damping constant $\alpha = 0.01$. An external magnetic field $B_z = 30$ mT was applied along the z-axis, with periodic boundary conditions imposed along all three spatial directions (x, y, z). Demagnetization effects were explicitly disabled.

The system's resonant modes were initially characterized using standard ferromagnetic resonance (FMR) procedures, enabling identification of both $+\mathcal{Q}$ and $-\mathcal{Q}$ spin-wave modes. Subsequent long-duration simulations ($> 500\,\mathrm{ns}$) under continuous microwave excitation in the range $0.01 \leq B \leq 0.3$ mT revealed the emergence of Archimedean screw-like textures. By systematically varying the microwave power, the frequency–power relationship of the screw dynamics was extracted. The associated phase-winding patterns were analyzed using time-resolved magnetization snapshots.

To study the role of disorder, we introduced a statistical defect model with a 0.01% vacancy concentration (8 sites in the $20 \times 20 \times 200$ lattice) by setting $M_s = 0$ and $\alpha = 0$ at the defect sites. Multiple random configurations were simulated to ensure statistical robustness. Each simulation followed a consistent protocol:

1. FMR characterization to determine $+\mathcal{Q}$ and $-\mathcal{Q}$ resonance frequencies;
2. Long-duration microwave excitation at the respective resonance;
3. Measurement of screw texture frequency as a function of input power.

S2. REAL-TIME MAGNETIZATION RESPONSE

Based on helimagnon theory and micromagnetic simulations, the two magnon modes, $\pm\mathcal{Q}$, arising from the conical spin order, can be expressed as:

$$\mathbf{m}(z,t) = \begin{pmatrix} \cos(2\pi q_h z + \phi) & -\sin(2\pi q_h z + \phi) & 0 \\ \sin(2\pi q_h z + \phi) & \cos(2\pi q_h z + \phi) & 0 \\ 0 & 0 & 1 \end{pmatrix} \begin{pmatrix} \cos\eta & 0 & \sin\eta \\ 0 & 1 & 0 \\ -\sin\eta & 0 & \cos\eta \end{pmatrix} \cdot \begin{pmatrix} \sin\xi & \cos(2\pi\omega_\pm t \pm 2\pi q_h z) \\ \sin\xi & \sin(2\pi\omega_\pm t \pm 2\pi q_h z) \\ & \cos\xi \end{pmatrix} \ , \tag{S1}$$

where ϕ is the static phase of the helix, η is the cone angle, ξ is the precession amplitude during resonance, q_h is the propagation vector of the helix, and $\omega_\pm$ the frequency applied to the conical spin helix for driving the system into the $\pm\mathcal{Q}$ magnon mode. Therefore, if the number of probed spins is sufficiently large, the real-time magnetization response can be written as

$$M_x(t) = \int_0^\infty dz\ m_x(z,t) \approx \int_0^{\lambda_h} dz\ m_x(z,t) \ , \tag{S2}$$

where $\lambda_h = 1/q_h = 60$ nm is the real-space pitch of the helix.

Inserting equation (S1) into equation (S2) yields a well-defined sinusoidal function for $M_x(t)$:

$$M_x(t) = \mathcal{A}_\pm \cos[2\pi\omega_\pm t + \phi_\pm] \ , \tag{S3}$$

where $\mathcal{A}_\pm$ is a constant amplitude, and $\phi_\pm$ is determined by the static phase ϕ.

To gain intuitive understanding of the relationship between the temporal phase $\phi_\pm$ and the static spatial phase ϕ, Fig. S1 shows numerically calculated $M_x(t)$ functions at the stationary $+\mathcal{Q}$ and $-\mathcal{Q}$ resonance states, based on equivalent conical spin structures with varying values of ϕ (see Fig. S1a,d). As shown in Fig. S1b,e, for both $+\mathcal{Q}$ and $-\mathcal{Q}$ modes, a structural phase shift in ϕ does not affect the amplitudes $\mathcal{A}_+$ and $\mathcal{A}_-$. However, the temporal phase ϕ_+ increases linearly with ϕ, while ϕ_- decreases linearly with ϕ, as demonstrated in Fig. S1c,f. These results provide a direct interpretation of equation (S3).

Importantly, when the conical chain undergoes an Archimedean screw motion at $|\mathbf{H}_{\rm rf}| \geq H_{\rm rf}^{\rm C}$, the structural phase becomes time-dependent, i.e.,

$$\phi = \pm 2\pi\Omega_\pm t \ . \tag{S4}$$

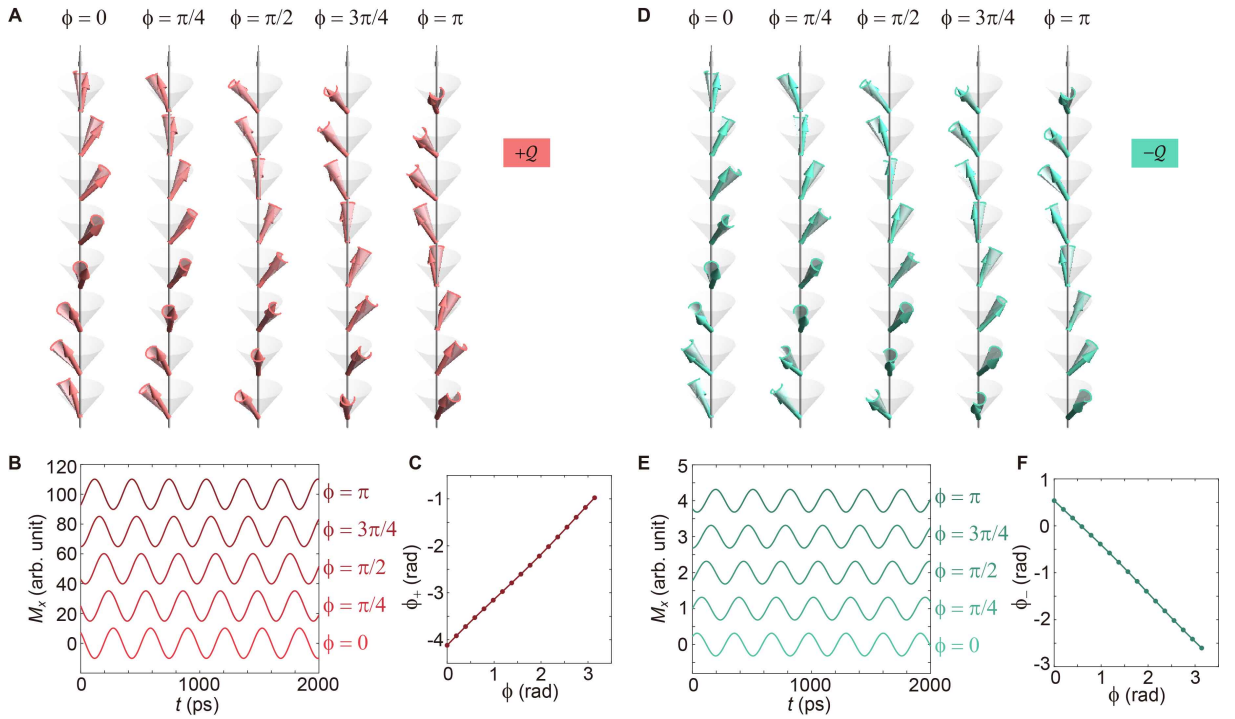

FIG. S1. At the stationary spin resonance state ($|\mathbf{H}_{\rm rf}| < H_{\rm rf}^{\rm C}$), the calculated $M_x(t)$ profiles are shown as a function of the conical structural phase ϕ. **a,b**, For the $+\mathcal{Q}$ mode, when the spin precession amplitude remains constant, a shift $\phi \to \phi + \delta\phi$ results in a linear phase shift of the $M_x(t)$ signal, such that $\phi_+ \to \phi_+ + \delta\phi$. **c**, This establishes a one-to-one correspondence between ϕ_+ and the underlying structural phase ϕ. **d-f**, Analogous results for the stationary $-\mathcal{Q}$ mode, corresponding to panels **a-c**.

Equation (S4) captures the essence of chiral phason dynamics. Substituting equation (S4) into equation (S3) yields equation (1) in the main text:

$$M_x(t) = \mathcal{A}_\pm \cos[2\pi(\omega_\pm \pm \Omega_\pm)t + \phi_\pm] \ . \tag{S5}$$

S3. STROBOSCOPIC MOKE DETECTION

The experimental setup, including the beam paths and microwave circuitry, is shown in Fig. 2a of the main text. It is important to note that at any transient time t, the measured polar MOKE signal is proportional to $M_x(t)$. To detect this transient response, an amplitude-modulation lock-in technique is employed. Specifically, the output microwave signal ($\omega_0 = 3.2$ GHz) is modulated by a local oscillator (LO) at a frequency of 1.237 kHz, which alternates the signal between on and off states. This LO signal is then used as the reference for lock-in detection by the avalanche photodiode (APD), yielding the stroboscopic signal denoted as S.

Thus, at a fixed time delay t_d, the measured $S(t_d)$ signal corresponds to the intensity difference between the microwave-on and microwave-off states. During the microwave-off cycles, the static conical structure is described by $m_0^x(z) = \sin\eta\cos(q_h z + \phi)$. For a conical chain with a sufficiently large number of spins, the spatially averaged magnetization satisfies $M_x = \int dz\ m_0^x(z) \approx 0$. In other words, the S signal effectively measures the time-integrated MOKE response while the microwave is on, i.e.,

$$S(t_d) = \sum_{n=1}^{N} M_x(n\Gamma_{\rm rep} + t_d) \ , \tag{S6}$$

where N is the number of laser pulses within each microwave-on cycle, which equals 64,673 for the present LO frequency. Accordingly, the measured $S(t_d)$ signal can be expressed explicitly as

$$\begin{aligned} S(t_d) &= \mathcal{A}_\pm \sum_{n=1}^{N} \cos[2\pi(\omega_\pm \pm \Omega_\pm)(n\Gamma_{\rm rep} + t_d) + \phi_\pm] \\ &= \frac{\mathcal{A}_\pm \sin[N\pi(\omega_\pm \pm \Omega_\pm)\Gamma_{\rm rep}]}{\sin[\pi(\omega_\pm \pm \Omega_\pm)\Gamma_{\rm rep}]} \cos[2\pi(\omega_\pm \pm \Omega_\pm)t_d + (N+1)\pi(\omega_\pm \pm \Omega_\pm)\Gamma_{\rm rep} + \phi_\pm] \ . \end{aligned} \tag{S7}$$

S4. SUPPLEMENTARY MOVIES

1. Supplementary Movie 1: The real-time dynamics for the backward-sliding phason that is activated by the $+\mathcal{Q}$ mode.

2. Supplementary Movie 2: The real-time dynamics for the forward-sliding phason that is activated by the $-\mathcal{Q}$ mode.